THE JOURNAL OF BIOLOGICAL CHEMISTRY VOL. 285, NO. 26, pp. 19997–20005, June 25, 2010

Effective Blockage of Both the Extrinsic and Intrinsic Pathways of Apoptosis in Mice by TAT-crmA

Received for publication, March 15, 2010, and in revised form, April 19, 2010 Published, JBC Papers in Press, April 28, 2010, DOI 10.1074/jbc.M110.122127

Stefan Krautwald[‡], Ekkehard Ziegler[‡], Lars Rölver[‡], Andreas Linkermann[‡], Kirsten A. Keyser[‡], Philip Steen[‡], Kai C. Wollert[§], Mortimer Korf-Klingebiel[§], and Ulrich Kunzendorf[‡1]

From the [‡]Division of Nephrology and Hypertension, University of Kiel, 24105 Kiel and the [§]Department of Cardiology and Angiology, Hannover Medical School, 30625 Hannover, Germany

Evidence accumulates that in clinically relevant cell death, both the intrinsic and extrinsic apoptotic pathway synergistically contribute to organ failure. In search for an inhibitor of apoptosis that provides effective blockage of these pathways, we analyzed viral proteins that evolved to protect the infected host cells. In particular, the cowpox virus protein crmA has been demonstrated to be capable of blocking key caspases of both pro-apoptotic pathways. To deliver crmA into eukaryotic cells, we fused the TAT protein transduction domain of HIV to the N terminus of crmA. *In vitro*, the TAT-crmA fusion protein was efficiently translocated into target cells and inhibited apoptosis mediated through caspase-8, caspase-9, and caspase-3 after stimulation with α-Fas, etoposide, doxorubicin, or staurosporine. The extrinsic apoptotic pathway was investigated following α-Fas stimulation. *In vivo* 90% of TAT-crmA-treated animals survived an otherwise lethal dose of α-Fas and showed protection from Fas-induced organ failure. To examine the intrinsic apoptotic pathway, we investigated the survival of mice treated with an otherwise lethal dose of doxorubicin. Whereas all control mice died within 31 days, 40% of mice that concomitantly received intraperitoneal injections of TAT-crmA survived. To test the ability to comprehensively block both the intrinsic and extrinsic apoptotic pathway in a clinically relevant setting, we employed a murine cardiac ischemia-reperfusion model. TAT-crmA reduced infarction size by 40% and preserved left ventricular function. In summary, these results provide a proof of principle for the inhibition of apoptosis with TAT-crmA, which might provide a new treatment option for ischemia-reperfusion injuries.

Apoptotic processes are centrally involved during organogenesis in complex organisms but may also cause organ failure in response to a variety of harmful stimuli. Certain infectious diseases, intoxications, or fulminant immune responses may trigger an overwhelming apoptotic response (1). Moreover, minimizing apoptotic organ failure due to ischemia-reperfusion injuries that occur during stroke or myocardial infarction remains a major challenge in clinical settings. Each year, ~1.5 million myocardial infarction cases are recorded in the United States. Myocardial infarction is the leading cause of death in both Europe and the United States. Therefore, transient blockage of apoptosis is of clinical importance to protect cardiac function and to save lives.

Apoptosis is controlled by the extrinsic death receptor pathway and the intrinsic mitochondrial pathway. Notably, both pathways converge at caspase-3, leading to activation of other proteases. Caspases have more than 400 different substrates that interfere with transcription, translation, DNA cleavage, cytoskeleton assembly, and membrane trafficking. To prevent this "death by a thousand cuts," it is important to block caspases in both the intrinsic and extrinsic pathways as well as caspases involved in the execution process of apoptosis (2). The extrinsic death receptor pathway is triggered by Fas-Fas ligand (FasL)[2] or tumor necrosis factor (TNF)-TNF-receptor ligation and proceeds through caspase-8 to activate executor caspases through caspase-3 (2). The intrinsic pathway is triggered, for example, through application of the DNA-damaging topoisomerase inhibitors doxorubicin, etoposide, and staurosporine, UV-radiation, glucocorticoids, endoplasmic reticulum stress, or serum growth factor deprivation (1, 2). Activation of this pathway involves mitochondrial outer membrane permeabilization, resulting in the release of cytochrome *c* from mitochondria, apoptosome assembly, and activation of caspase-9 and caspase-3 (2, 3). Doxorubicin-induced organ damage was recently shown to depend exclusively on the intrinsic apoptotic pathway and was prevented by the CO/heme oxygenase system (4). However, both pathways are known to interact, because isomerase inhibitors cleave the BH3-only protein Bid, which in turn triggers the intrinsic apoptotic pathway independently of caspase-8 and exhibits a feed-forward amplification loop through caspase-3 (5). These inhibitors are thus suitable agents for investigating the intrinsic pathway.

The cowpox virus serpin crmA inhibits the initiator caspases of the extrinsic pathway, caspase-8 and -10, caspase-9 of the intrinsic pathway, and the executor caspases-3 and -6 (6–9). Fusion of an intracellularly acting protein to a protein transduction domain has been shown to be sufficient for ensuring its entry into mammalian cells. Several protein transduction domains have been tested, but derivatives of the transactivator of transcription (TAT) domain of HIV have proven to be the

[1] To whom correspondence should be addressed: University Kiel, Division of Nephrology and Hypertension, Schittenhelmstrasse 12, 24105 Kiel, Germany. Tel.: 49-431-597-1336; Fax: 49-431-597-1337; E-mail: kunzendorf@nephro.uni-kiel.de.

[2] The abbreviations used are: FasL, Fas ligand; TAT, transactivator of transcription; TNF, tumor necrosis factor; HIV, human immunodeficiency virus; H&E, hematoxylin and eosin; TUNEL, terminal deoxynucleotidyl transferase-mediated dUTP nick end labeling; DAPI, 4′,6-diamidino-2-phenylindole; LVEDV, left ventricular end-diastolic volume; LVESV, left ventricular end-systolic volume; GFP, green fluorescent protein.

most effective. The delivery of a variety of proteins into all tissues in mice, including passage across the blood-brain barrier, and the safety of the TAT domain have been demonstrated in detail (10, 11).

In clinically relevant cell death, both the intrinsic and extrinsic apoptotic pathways synergistically contribute to organ failure. In fulminant liver failure, renal ischemia-reperfusion, myocardial infarction, various intoxications and stroke, and activation of caspase-3, caspase-8, and caspase-9 have been suggested (1).

In the pathophysiology of organ ischemia, reperfusion injury accounts for up to 50% of the final infarction size and is accompanied by mitochondrial calcium overload and ATP depletion, which are associated with the opening of mitochondrial permeability transition pores at the inner mitochondrial membrane (12). Collapse of the mitochondrial membrane potential ($\Delta\Psi$) results in release of cytochrome *c* into the cytosol, initiating the intrinsic apoptotic pathway. Above this, receptor-mediated apoptosis has been extensively investigated in ischemia-reperfusion injury. TNF-receptor- and FasL-deficient mice are protected from ischemia-reperfusion injury in various organs, *e.g.* kidney, brain, and liver (13–15). Therefore, a promising blocker of apoptosis ought to inhibit both the intrinsic and extrinsic apoptotic pathway.

Herein we demonstrate that the fusion protein TAT-crmA is capable of effectively blocking both the intrinsic and extrinsic apoptotic pathways *in vitro* and *in vivo*. Finally, the comprehensive anti-apoptotic impact of TAT-crmA is highlighted by the reduction of infarct size and preservation of the left ventricular ejection fraction in a mouse model of myocardial infarction.

EXPERIMENTAL PROCEDURES

Cloning, Expression, and Purification of TAT-crmA—Total RNA was isolated from human skin lesions caused by cowpox virus using RNeasy minicolumns (Qiagen). cDNA was generated using the Thermoscript RT-PCR System (Invitrogen) with forward (5′-CCGGGTACCGATATCTTCAGGGAAATCGCATC-3′) and reverse (5′-CCGGAATTCTTAATTAGTTGTTGGAGAGCAATATCTA-3′) primers.

The pTAT vector has an N-terminal 6-histidine leader, followed by the 11-amino acid TAT protein transduction domain and a polylinker. The PCR product was cloned into a KpnI/EcoRI-cut pTAT-vector. The resulting construct from a selected colony harboring the cDNA of TAT-crmA was transformed into competent T7 Express *Escherichia coli* bacteria (New England BioLabs, Frankfurt, Germany) and induced in LB media with isopropyl-β-D-thiogalactopyranoside (final concentration of 0.4 mM). After incubation for 3 h at 37 °C, cells were harvested by centrifugation (6,500 × *g*, 10 min, 4 °C) followed by sonication in binding buffer (300 mM NaCl, 50 mM sodium phosphate, pH 7.0). Suspensions were clarified by centrifugation (14,000 × *g*, 20 min, 4 °C), and supernatants containing TAT proteins were purified under native conditions using pre-equilibrated TALON™ Metal Affinity Resin (Clontech-Takara Bio Europe, St. Germain-en-Laye, France). To remove background of contaminating bacterial proteins, columns were washed by stepwise additions of increasing imidazole concentrations. Finally, target proteins were eluted with an elution buffer containing 300 mM NaCl, 50 mM sodium phosphate, and 150 mM imidazole (pH 7.0). Removal of salt was performed using a disposable PD-10 (Sephadex G-25) desalting column equilibrated with RPMI medium supplemented with 0.026% albumin. Fusion protein was either used immediately after purification or stored at −20 °C. To control quality and confirm quantification, protein samples were analyzed by gel electrophoresis.

Cell Culture and Immunoblotting—The human lymphocytic Jurkat cells (ATCC, Manassas, VA) were cultured in RPMI medium supplemented with 10% fetal calf serum and penicillin-streptomycin. For experiments, cells were seeded at a density of 1×10^6 cells/ml. Investigation of α-Fas-, staurosporine-, etoposide-, and doxorubicin-induced apoptosis was performed by preincubating cells with the TAT fusion protein (500 nM) for 5 min prior to addition of various stimuli for different time periods. For immunoblotting, cells were lysed in ice-cold 10 mM Tris-HCl, pH 7.5, 50 mM NaCl, 1% Triton X-100, 30 mM sodium pyrophosphate, 50 mM NaF, 100 μM Na_3VO_4, 2 μM $ZnCl_2$, and 1 mM phenylmethylsulfonyl fluoride (modified Frackelton buffer). Insoluble material was removed by centrifugation (14,000 × *g*, 10 min, 4 °C), and protein concentration was determined using a commercial Bradford assay kit according to the manufacturer's instructions (Bio-Rad).

Equal amounts of protein (20 μg/lane) were resolved on SDS-PAGE gels and transferred to nitrocellulose membranes (Amersham Biosciences). Western blots were performed using a monoclonal α-crmA antibody (BD Biosciences), a polyclonal α-cleaved caspase-3 antibody (Asp-175), a monoclonal α-caspase-8 antibody (1C12), or a polyclonal α-cleaved caspase-9 antibody (human specific Asp330 and mouse specific Asp353; all from New England Biolabs) and a corresponding secondary horseradish peroxidase-linked α-mouse or α-rabbit antibody (both from Promega, Madison, WI). Immune complexes were visualized by enhanced chemiluminescence (ECL, Amersham Biosciences).

Annexin V Staining—Apoptosis was quantified by Annexin V staining and fluorescence-activated cell sorting analysis. After stimulation of Jurkat cells with α-human Fas (clone 7C11, Immunotech, Marseille, France) for 4 h, cells were harvested and washed with RPMI supplemented with 2% fetal calf serum. Annexin V staining (ApoAlert, Annexin V-FITC, BD Biosciences) was performed according to the manufacturer's instructions. Fluorescence was analyzed using an EPICS XL® (Coulter, Krefeld, Germany) flow cytometer. Data were analyzed using the EPICS System II software.

Spectrofluorometric Analysis of Caspase Activity—For fluorometric caspase assays, stimulation of cells (α-Fas alone or with TAT-crmA for indicated times) was terminated by aspirating the medium and washing the cells twice with ice-cold phosphate-buffered saline. Cells were resuspended in cold cell lysis buffer (BD Biosciences) and kept on ice for 30 min. Cell lysates were incubated with caspase substrate and analyzed by spectrofluorometry.

Analysis of Changes in Mitochondrial Membrane Potential—The mitochondrial outer membrane permeabilization transition event, an early indicator of cellular apoptosis, was measured by detecting changes in membrane potential ($\Delta\Psi$).

Briefly, loss of Ψ was determined by a decrease of fluorescence of the cationic dye 5,5′,6,6′-tetra-chloro-1,1′,3,3′-tetraethyl-benzamidazolocarbo-cyanin iodide that no longer accumulates inside the mitochondria upon collapse of the Ψ. For detection of the fluorescence intensity, an excitation wavelength of 490 nm and an emission wavelength of 527 nm were used. The efficacy of TAT-crmA after induction of apoptosis in response to different stimuli was tested using the Mito-PT^{TM} kit according to the manufacturer's instructions (Immunochemistry Technologies, LLC, Bloomington, MN).

In Vivo Detection of Apoptosis—Female BALB/c mice were purchased from Charles River (Sulzfeld, Germany) and used for experiments at 6–8 weeks of age. Apoptosis was induced by intraperitoneal injection of monoclonal agonistic α-Fas antibody Jo2 (1 mg/kg body weight) or doxorubicin (15 mg/kg body weight). For survival studies 10 mice per group received α-Fas monoclonal antibody Jo2 and 5 mice per group received doxorubicin either alone or in combination with TAT-crmA. Injection of 150 μg of TAT-crmA or vehicle was performed intraperitoneally 20 min and 5 min prior to application of Jo2 monoclonal antibody or doxorubicin. For histological cryosection (5 μm) analysis, treated mice (1 mg of Jo2/kg body weight or 80 mg of doxorubicin/kg body weight) were sacrificed 5 or 8 h after injection of Jo2 monoclonal antibody to harvest livers or 6 h after application of doxorubicin to excise hearts. Sections were fixed with acetone, stained for 1 min with hematoxylin and eosin (H&E) and examined by light microscopy at 200× and 400× magnification. Apoptotic cells were identified in paraformaldehyde-fixed organ sections (5 μm) using terminal deoxynucleotidyl transferase-mediated dUTP nick end labeling (TUNEL, In Situ Cell Death Detection Kit, TMR red, Roche Molecular Biochemicals, Mannheim, Germany). Staining was performed according to the manufacturer's instructions. TUNEL-positive cells were visualized by fluorescence microscopy at 200× and 400× magnification. Nuclei were counterstained with DAPI (Dianova, Hamburg, Germany).

Myocardial Ischemia-Reperfusion Model—Twelve-week-old male C57BL/6 mice were anesthetized with ketamine hydrochloride (100 mg/kg, intraperitoneally) and xylazine (4 mg/kg, intraperitoneally). After tracheal intubation, anesthesia was maintained with 2% isoflurane. Mice underwent transient coronary artery ligation for 1 h, followed by reperfusion for 24 h. Area at risk and infarction sizes were determined by Evans blue and 2,3,5-triphenyltetrazolium chloride staining and computerized planimetry as previously described (16). Transthoracic echocardiography was performed with a linear 15-MHz transducer in mice sedated with 2% isoflurane. Long axis images (to determine left ventricular end-diastolic volume (LVEDV) and left ventricular end-systolic volume (LVESV)) and M-mode tracings were recorded. Ejection fraction was calculated as [(LVEDV − LVESV)/LVEDV] × 100.

RESULTS

Production of TAT-crmA Fusion Protein—To develop a comprehensive inhibitor of apoptosis we generated the cowpox virus serpin crmA in a cell-permeable recombinant form by fusing it to the TAT domain of HIV. The coding cDNA sequence of crmA was cloned into a pTAT bacterial expression vector that contains an N-terminal TAT protein transduction domain leader followed by a polylinker (10). We purified this protein under native conditions and verified its biological effectiveness. Initially, we addressed its permeability by incubating human lymphocytes with TAT-crmA. Concentration-dependent transduction of the recombinant protein was shown by Western blot analysis of whole cell lysates (Fig. 1*A*). TAT-crmA was detectable at a final concentration of 125 nM and reached a plateau at 500 nM. For all subsequent experiments, we chose a concentration of 500 nM to deliver sufficient amounts of fusion protein into the cells. As demonstrated in Fig. 1*B*, lymphocytes were incubated for different durations, and TAT-crmA was added in serum-free media at a final concentration of 500 nM. Time-dependent uptake of TAT-crmA was determined in whole cell lysates by immunoblotting with a monoclonal α-crmA antibody. Maximal intracellular presence was detected within 10 min of incubation at 37 °C. After 30 min the concentration of TAT-crmA decreased slowly but remained detectable for >3 h. These data are consistent with the kinetics of other previously published TAT proteins (17).

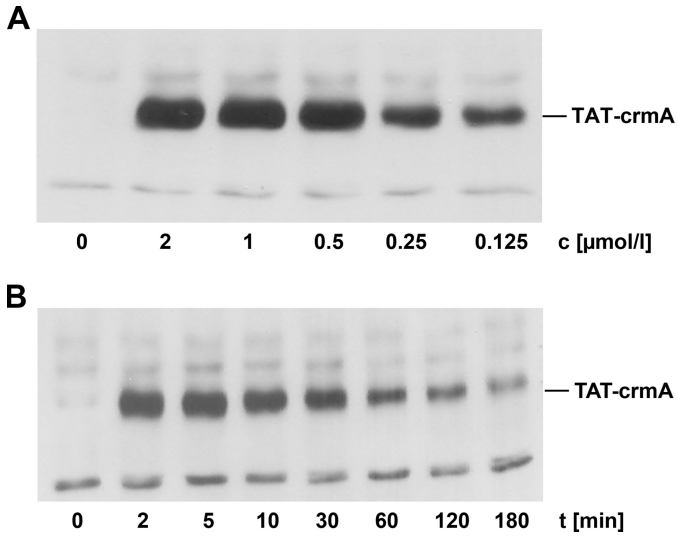

FIGURE 1. **Transducibility and availability of TAT-crmA *in vitro*.** *A*, Jurkat cells were incubated for 5 min at 37 °C with different concentrations of TAT-crmA. Stimulation was terminated, cells were lysed, insoluble material was removed, and protein concentrations were determined. Equal amounts of protein (20 μg/*lane*) were resolved by SDS-PAGE and transferred onto nitrocellulose membranes for immunoblotting. Transduced TAT fusion protein is detected with an α-crmA antibody. *B*, Jurkat cells were incubated for the indicated times with 500 nM TAT-crmA at 37 °C and processed as above.

TAT-crmA Inhibits Activation of the Extrinsic Apoptotic Pathway in Vitro—We demonstrated the ability of transduced recombinant TAT-crmA to inhibit the extrinsic apoptotic pathway induced by α-human Fas antibody (7C11) in Jurkat cells and assessed the level of apoptotic cells by flow cytometry. Four hours after stimulation with α-Fas, cells incubated concomitantly with 500 nM TAT-crmA were protected from extrinsic apoptosis, as demonstrated by umarin reduction in Annexin V-positive cells (Fig. 2*A*). As shown in Fig. 2*B* TAT-crmA reduced the cleavage of procaspase-8 in Jurkat cells in response to α-human Fas treatment in a time-dependent manner. Increased concentrations of cleaved caspase-8 subunits (p43/41 and a smaller fragment of ~18 kDa) were visible after 3–7 h. Preincubation with 500 nM TAT-crmA fusion protein

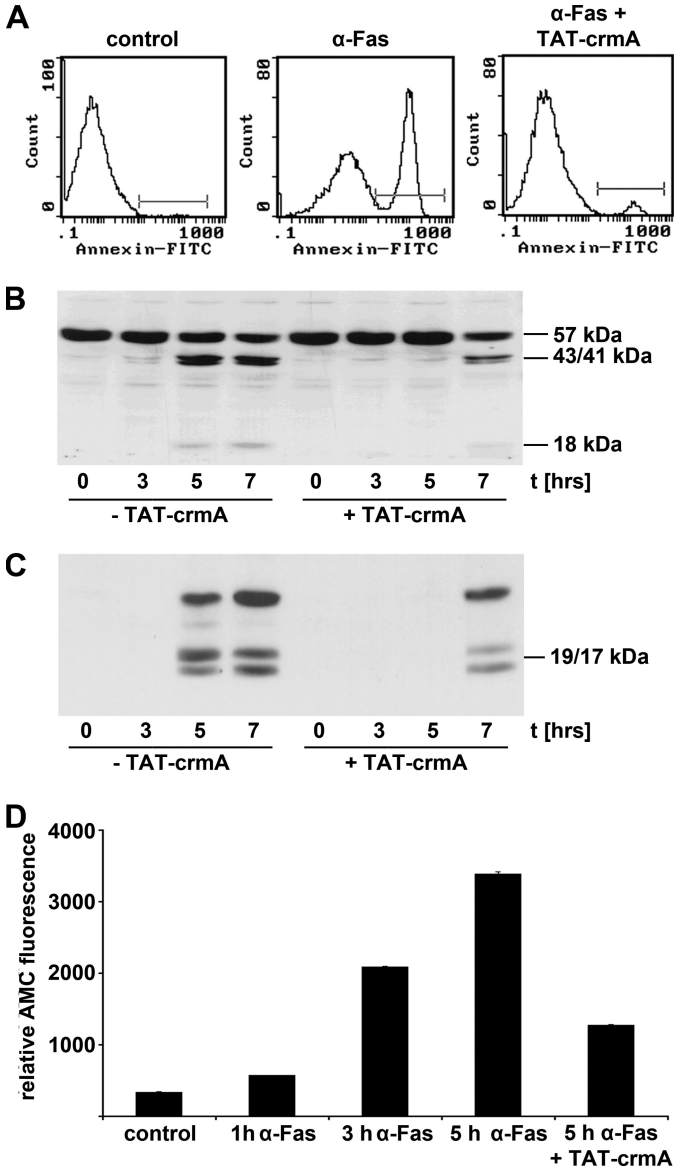

FIGURE 2. **TAT-crmA inhibits activation of the extrinsic apoptotic pathway *in vitro*.** *A*, Jurkat cells were incubated with either 100 ng/ml α-Fas (7C11) for 4 h at 37 °C alone (*middle*) or for 5 min with 500 nM TAT-crmA followed by 100 ng/ml α-Fas (*right*). Untreated cells were incubated with vehicle (*left*). Detection of apoptosis was performed by fluorescence-activated cell sorting analysis using an Annexin V-FITC antibody. The *graphs* show the results of a representative experiment. *B*, caspase-8 activation 3, 5, and 7 h after α-Fas stimulation (100 ng/ml) of Jurkat cells with or without 500 nM TAT-crmA. The band at 57 kDa shows procaspase-8 and bands at 43/41 and 18 kDa indicate cleaved, active caspase-8. Although control cells showed high levels of active caspase-8 after 3–5 h, TAT-crmA reduced this intensity and decelerated the time course of the extrinsic apoptotic pathway. *C*, TAT-crmA-mediated reduction of caspase-3 activity in Jurkat cells. Compared with cells treated with 100 ng/ml α-Fas alone, TAT-crmA-treated Jurkat cells did not activate caspase-3 after 5 h. However, 7 h after stimulation, active caspase-3 was detected in fusion protein-treated cells. *D*, functional anti-apoptotic effect of TAT-crmA in α-Fas-activated Jurkat cells. Relative fluorescence increased within the first 5 h after addition of α-Fas. Upon co-incubation with 500 nM TAT-crmA, protease activity of caspase-8 was significantly reduced after 5 h.

for 5 min completely blocked cleavage of procaspase-8 for at least 5 h and resulted in significantly reduced activation after 7 h. We further analyzed the activity of caspase-3 (Fig. 2*C*). When caspase-8 activates caspase-3, it cleaves the fluorogenic substrate Ac-DEVD-7-amino-4-methylcoumarin. Following co-incubation of α-Fas-treated Jurkat cells with 500 nM TAT-crmA, the protease activity of caspase-3 was reduced by >60% after 5 h (Fig. 2*D*).

TAT-crmA Inhibits Activation of the Extrinsic Apoptotic Pathway in Vivo—The principle capacity of TAT fusion proteins to transduce into murine liver cells *in vivo* was assured by using a GFP-tagged TAT fusion protein. This was detectable in liver micrographs 5 min after intravenous injection of 250 μg into mice (Fig. 3*A*). Consequently, mice received intraperitoneal injections of 1 mg/kg body weight α-Fas monoclonal antibody (Jo2) alone or in combination with 7.5 mg/kg body weight TAT-crmA fusion protein. For histological analyses, mice were sacrificed 5 or 8 h after α-Fas injection. Macroscopically, the liver appeared dark brown in α-Fas-treated animals, but concomitant application of TAT-crmA preserved the normal appearance of the organ (Fig. 3*B*). These observations were substantiated by histological evaluation (Fig. 3*C*). H&E-stained liver tissue exhibited severe liver cell death 5 and 8 h after α-Fas treatment that was prevented by co-treatment with TAT-crmA. TUNEL staining revealed an absence of apoptosis in TAT-crmA-treated animals (Fig. 3*D*). Survival after an otherwise lethal dose of α-Fas was prolonged throughout the entire observation period of 3 months. Although 100% of control mice died within 7 h of α-Fas injection, only a single TAT-crmA-treated mouse died 14 h after injection ($n = 10$, $p < 0.001$, Fig. 3*E*).

TAT-crmA Inhibits Activation of the Intrinsic Apoptotic Pathway in Vitro—To analyze the ability of TAT-crmA to inhibit the intrinsic apoptotic pathway *in vitro*, we measured mitochondrial $\Delta\Psi$, an early event of the intrinsic apoptotic pathway. Changes in mitochondrial $\Delta\Psi$ in Jurkat cells after stimulation with topoisomerase inhibitors staurosporine (2.5 μM) for 2 h or etoposide (100 μM) for 24 h are shown in Fig. 4*A*. Loss of mitochondrial $\Delta\Psi$ was reproducibly blocked by concomitant treatment of 500 nM TAT-crmA in either staurosporine- or etoposide-treated cells. The number of apoptotic cells in the fusion protein-treated group was reduced by ~80% in staurosporine-treated cells ($p < 0.02$) and by 50% in etoposide-treated cells ($p < 0.05$). When mitochondrial $\Delta\Psi$ declines, mitochondria release cytochrome *c*, thereby initiating the assembly of the apoptosome, which includes activated caspase-9. The cleaved 37-kDa fragment of caspase-9 was detected by Western blotting of Jurkat cells treated with 10 μM doxorubicin, another topoisomerase inhibitor (Fig. 4*B*). Therein, we show that addition of 500 nM TAT-crmA effectively suppressed cleavage of caspase-9.

TAT-crmA Inhibits Activation of the Intrinsic Apoptotic Pathway in Vivo—The *in vivo* transducibility of TAT-GFP into cardiomyocytes was confirmed after intravenous injection of 250 μg of fusion protein. Mice were sacrificed 5 min after injection, and the heart was excised for histological evaluation. Nuclei were counterstained with DAPI (*blue*), and autofluorescence of myocardiocytes appears *red* (Fig. 5*A*). To evaluate the effects of TAT-crmA on the intrinsic apoptotic pathway *in vivo*, BALB/c mice were treated with a single intraperitoneal injection of 80 mg/kg body weight doxorubicin with or without two doses of 15 mg/kg body weight TAT-crmA 20 min and 5 min before the doxorubicin injection. The high stimulus concentra-

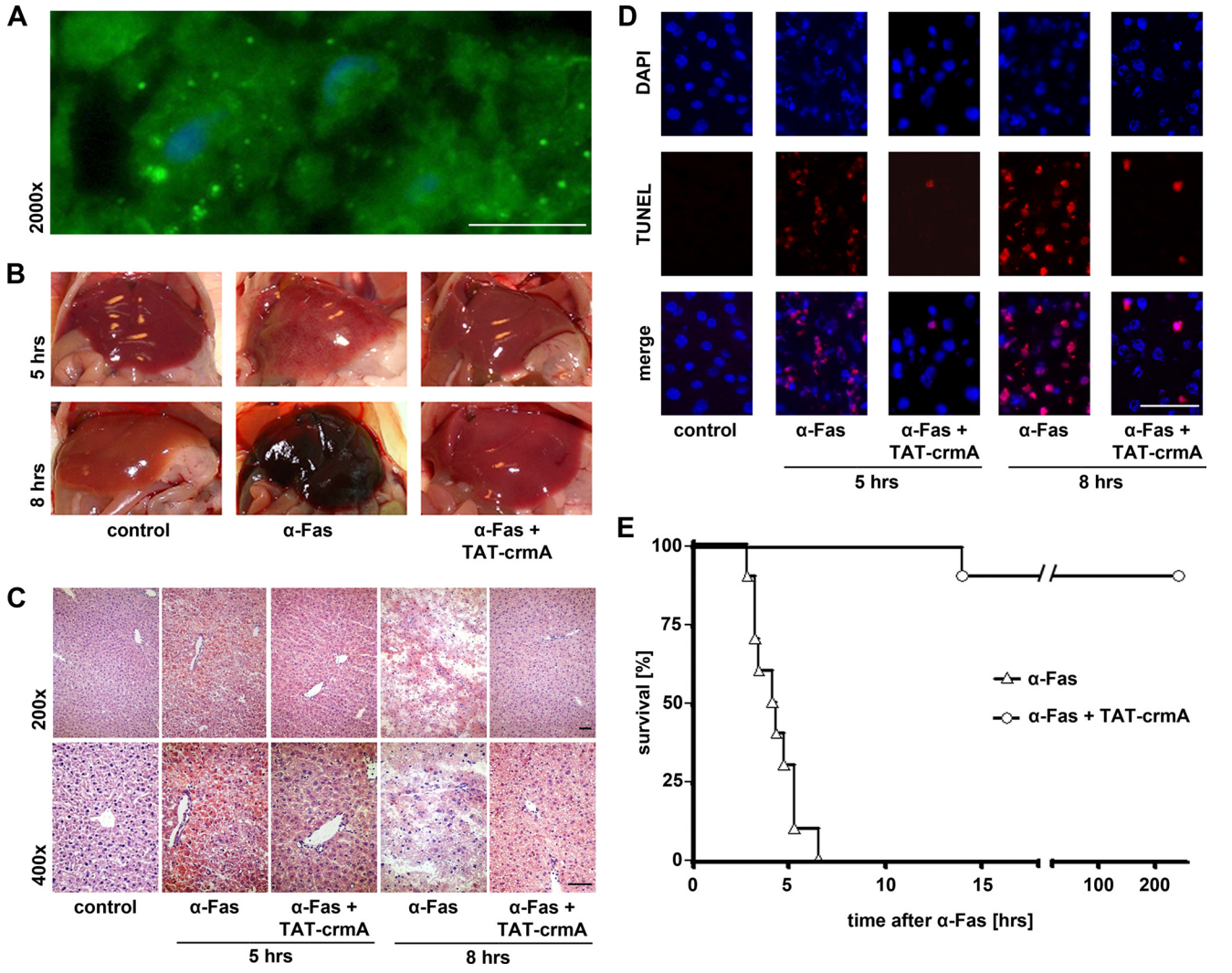

FIGURE 3. **The induction of the extrinsic apoptotic pathway is significantly suppressed *in vivo* after treatment with TAT-crmA.** *A*, confirmation of *in vivo* transducibility of TAT-GFP in hepatocytes. Mice were sacrificed 5 min after intravenous application of 250 μg of purified TAT-GFP protein, and livers were excised for cryosections. Successful transduction of purified TAT-GFP was observed by detection of green fluorescence. Nuclei were counterstained with DAPI (*blue*). *B*, macroscopic appearance of whole livers from mice that received 1 mg/kg body weight Jo2 alone or in combination with 7.5 mg/kg body weight TAT-crmA. Liver failure that was seen 5 and 8 h after α-Fas treatment was ameliorated by treatment with TAT-crmA. *C*, histological evaluation of liver damage by H&E staining. Micrographs at 200× (*upper*) and 400× (*lower*) magnification of control, Jo2-treated, and TAT-crmA-treated mice are shown. Substantial structural liver failure was prevented by intraperitoneal injection of TAT-crmA. *D*, TUNEL staining (*red*) of the same liver preparations, overlaid with DAPI-stained nuclei (*blue*), revealed a significantly diminished number of TUNEL-positive cells (*purple*) in TAT-crmA-treated mice compared with animals treated with α-Fas alone. *E*, survival after an otherwise lethal dose of α-Fas was significantly prolonged by a single intraperitoneal injection of TAT-crmA ($p < 0.001$). *Bars* represent 50 μm.

tion of doxorubicin was chosen to allow detection of capase-9 activation within 6 h. After this time, mice were sacrificed, hearts were homogenized and cell lysates were analyzed for activated caspase-9 by Western blot (Fig. 5*B*). Concomitant TAT-crmA treatment strongly decreased activation and cleavage of caspase-9 after doxorubicin injection, demonstrating the potent anti-apoptotic effect of TAT-crmA. Excised hearts were also TUNEL-stained, as depicted in Fig. 5*C*. Positive TUNEL staining of doxorubicin-treated mice was prevented by TAT-crmA treatment. Survival after an otherwise lethal dose of doxorubicin was prolonged with semi-daily applications of TAT-crmA for the first 7 days. Although all doxorubicin-treated mice died within 31 days, 40% of mice concomitantly treated with TAT-crmA survived ($n = 5$; Fig. 5*E*). Taken together, these results provide evidence for the efficient inhibition of both the intrinsic and extrinsic apoptotic pathways following TAT-crmA treatment *in vitro* and *in vivo*. The combination of the above shown results led us to examine the therapeutic potential of TAT-crmA in blocking apoptosis in a clinically relevant setting.

TAT-crmA Reduces Infarction Size and Improves Systolic Function after Myocardial Infarction in Mice—Because apoptosis of both the intrinsic and extrinsic pathways is a major pathophysiological event in ischemic tissues, we tested TAT-crmA in a murine myocardial infarction model. One hour after ischemia we analyzed the therapeutic efficacy of TAT-crmA, which was applied at the time of reperfusion. Infarction size in TAT-crmA-treated mice was reduced by ~40% (Fig. 6*A* and Table 1). These mice displayed an ejection fraction of 39.3 ± 4.2% compared with 23.2 ± 4.9% ($n = 13$, $p = 0.002$) in vehicle-treated mice. The LVESV decreased to 39.6% in TAT-crmA-treated mice from 53.3% in vehicle-treated animals ($p = 0,003$).

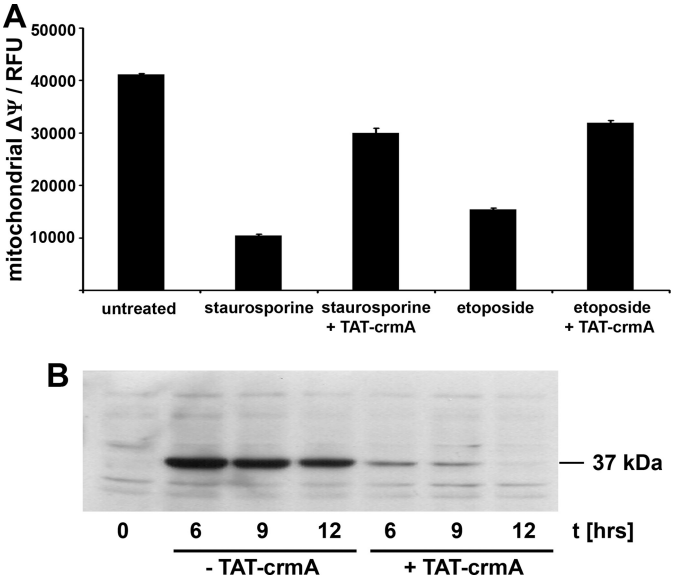

FIGURE 4. **TAT-crmA inhibits activation of the intrinsic apoptotic pathway *in vitro*.** *A*, changes in mitochondrial membrane potential ($\Delta\Psi$) of untreated, 2.5 μM staurosporine-treated (2 h), and 100 μM etoposide-treated (24 h) Jurkat cells. Induction of apoptosis was significantly reduced in both staurosporine-treated and etoposide-treated cells after incubation with 500 nM TAT-crmA fusion protein. *B*, activation of caspase-9 in Jurkat cells by stimulation with 10 μM doxorubicin for indicated times with or without treatment with 500 nM TAT-crmA. The band at 37 kDa shows cleaved caspase-9, which was not detectable in the untreated control. In contrast to cells stimulated with doxorubicin alone, TAT-crmA-treated Jurkat cells did not activate caspase-9 after 12 h. 6 and 9 h after doxorubicin stimulation active caspase-9 was only weakly detected in fusion protein-treated cells.

The LVEDV did not change significantly. Our results correspond with a significantly reduced LVESV in the TAT-crmA-treated group. H&E-stained cross-sections of the heart muscles of vehicle-treated mice showed typical myocardial infarction morphology, with vacuolization of cardiomyocytes, edema, and infiltration of granulocytes and mononuclear cells (Fig. 6*B*). These histological signs were significantly less pronounced in heart tissues obtained from TAT-crmA-treated mice. When apoptotic cardiomyocytes were detected by TUNEL staining, vehicle-treated mice showed more positivity in the infarction border zone after ischemia-reperfusion injury compared with TAT-crmA-treated littermates, indicating that crmA limits myocardial tissue damage *in vivo* (Fig. 6*C*). Thus, TAT-crmA functionally protects from myocardial ischemia-reperfusion injury.

DISCUSSION

Generally, there are two major apoptotic pathways: the death receptor-mediated (extrinsic) pathway and the mitochondria-mediated (intrinsic) pathway. Caspases are the key effector molecules in apoptosis and are potential targets for pharmacological modulation of cell death. Increased caspase activity is often observed at sites of cellular damage in a number of diseases, including stroke, sepsis, and myocardial infarction or is a common pathway that mediates toxicity of drugs. Inhibition of caspase activity in these diseases was predicted to be therapeutically beneficial. The discovery of drugs that selectively inhibit caspases should help to control such diseases, and proof-of-concept data have been obtained in several animal models (18, 19). Because of the extensive network between the intrinsic and extrinsic pathways (2), we propose that a recombinant protein that verifiably interacts with the apoptotic machinery at various stages of the apoptotic process outmatches highly specific synthetic caspase inhibitors. Indeed, many viruses express various caspase modulators that inhibit their activity by direct protein-protein interactions. Among these, the cowpox virus protein crmA is of particular interest, because it has the unique capacity to block both the intrinsic and extrinsic apoptotic pathway. Therefore, we created a fusion protein consisting of crmA and the HIV protein TAT to generate a potent anti-apoptotic molecule and demonstrate its ability to transduce in a concentration- and time-dependent manner into target cells (Fig. 1).

TAT-crmA inhibited the extrinsic apoptotic pathway induced by Fas/FasL ligation. CrmA-mediated reduction of caspase-8 activity *in vitro* (Fig. 2) gave rise to the *in vivo* experiments that demonstrated nearly complete protection from severe liver damage after α-Fas injection in the TAT-crmA-treated group (Fig. 3, *A–D*). The highly significant survival benefit observed in mice treated with TAT-crmA after α-Fas application underlines the extraordinary potential of crmA to inhibit the extrinsic pathway (Fig. 3*E*).

Activation of the intrinsic apoptotic pathway requires the activation of caspase-9. We found that caspase-9 lacked substantial cleavage activity following TAT-crmA co-incubation. *In vitro*, TAT-crmA protected cells from the collapse of mitochondrial $\Delta\Psi$ induced by various stimuli (Fig. 4*A*). This observation is explained by the presence of positive feedback loops in the pro-apoptotic signaling pathways. For example, it was shown that caspase-3, when activated through the intrinsic pathway, reactivates caspase-8 that in turn cleaves the Bid protein to activate mitochondria (20). Our data indicate that TAT-crmA functionally breaks down this feedback loop. The topoisomerase inhibitor doxorubicin uncouples electron transfer and oxidative phosphorylation in the mitochondria of cardiomyocytes, resulting in organ damage (4) and caspase-9 activation (Fig. 5*B*). TAT-crmA protected mice from doxorubicin-induced cardiomyopathy *in vivo* (Fig. 5*C*). Accordingly, we analyzed an established lethal mouse model of the intrinsic pathway employing a single injection of doxorubicin (4). A 40% survival rate after an otherwise lethal dose of doxorubicin was observed following TAT-crmA treatment (Fig. 5*D*). The significant survival benefit underlines the potential of TAT-crmA to inhibit the intrinsic pathway *in vivo*.

To evaluate the therapeutic potential of TAT-crmA in a setting that, like many clinically relevant situations, involves both the intrinsic and extrinsic apoptotic pathways, we characterized the effect of the fusion protein in a murine myocardial ischemia-reperfusion model. Expression of Fas and FasL are increased in hypoxic myocytes, and activation of Fas has been shown to induce apoptosis in cardiac myocytes (21, 22). However, mice with a functionally relevant mutation in the extracellular portion of Fas (*lpr* mice) or Fas ligand (*gld* mice) exhibited similar infarction sizes compared with wild-type mice (23, 24). In contrast, vanadyl sulfate treatment caused decreased expression of FasL, and this was correlated with reduced caspase-3 activation and reduced myocardial infarction *in vivo* (25). These controversial results require further research to reveal

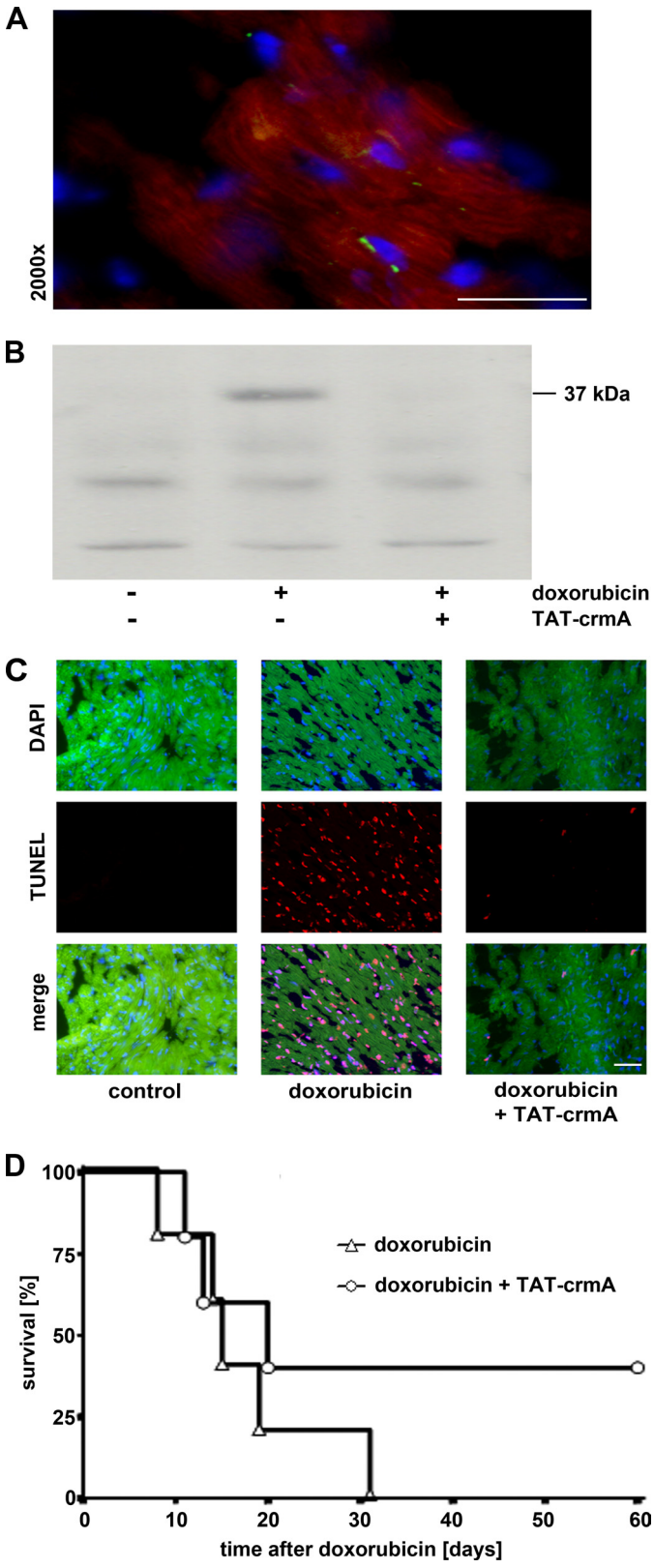

FIGURE 5. **Suppression of the intrinsic apoptotic pathway after treatment with TAT-crmA *in vivo*.** *A*, confirmation of *in vivo* transducibility of TAT-GFP in cardiomyocytes. Mice were sacrificed 5 min after intravenous application of 250 μg of purified TAT-GFP protein, and hearts were excised for cryosections. Successful transduction of purified TAT-GFP was observed by detection of green fluorescence. Nuclei were counterstained with DAPI (*blue*), and cells showed autofluorescence (*red*). *B*, doxorubicin-induced activation of caspase-9 was suppressed in mice after TAT-crmA injection. Animals were sacrificed 6 h after stimulation with 80 mg/kg doxorubicin and cleaved caspase-9 (37 kDa) in heart tissue protein lysates were detected by Western blot. Concomitant TAT-crmA treatment prevented activation and cleavage of caspase-9. *C*, cellular apoptosis within the same heart preparations was evaluated histologically by TUNEL staining (*red*). Images overlaid with DAPI-stained nuclei (*blue*) demonstrated that myocardial tissue apoptosis seen 6 h after treatment with a high dose of doxorubicin (80 mg/kg) was ameliorated by TAT-crmA treatment. *D*, survival after an otherwise lethal dose of doxorubicin (15 mg/kg body weight) was significantly prolonged by concomitant injections of TAT-crmA. *Bars* represent 50 μm.

the underlying pathophysiology in detail. Clinically, however, evidence accumulates concerning the importance of the intrinsic pathway in the pathophysiological course of myocardial infarction (1). We demonstrated that TAT-crmA effectively prevented apoptotic tissue damage caused by reperfusion injury following myocardial ischemia *in vivo* (Fig. 6, *A–C*).

The influence of hypoxia on life or death decisions is not exclusively pro-apoptotic but also induces a variety of protective endogenous activities in cardiomyocytes to prevent ischemic tissue damage, including the heme oxygenase-1-system, activation of phosphatidylinositol 3-kinase, initiation of the Akt pathway and up-regulation of nitric-oxide synthase. The efficacy of these protective mechanisms was demonstrated more than 20 years ago (26). Our *in vivo* results indicate that TAT-crmA treatment delays the onset of activation of a variety of caspases and inhibits death receptor-mediated and mitochondria-induced apoptosis (Figs. 3*E* and 5*D*). Mechanistically, it is tempting to speculate that the protein crmA decelerates the progression of ongoing cell death pathways, thereby providing time to activate the complex anti-apoptotic machinery in cells that are at risk to undergo any kind of programmed cell death. Therefore, transient inhibition of apoptosis by TAT-crmA during myocardial ischemia may provide time for cardiomyocytes to up-regulate these defense mechanisms. However, this hypothesis remains to be investigated in future studies.

The impressive potential of crmA inspired other researchers to investigate various approaches to potently inhibit apoptotic processes. However, the limited success of these studies might be explained by the way of delivery of crmA, *e.g.* stable transfection of target cells (27). Among others, Kilic *et al.* designed crmA transgenic mice that remained healthy and did not differ from wild-type mice in any of the evaluated parameters (28). When the crmA transgenic mice underwent stroke due to occlusion of the middle cerebral artery, no difference in infarction size could be detected compared with wild-type mice. This led the authors to conclude that crmA does not confer protection against ischemia-reperfusion injury. The results presented here contrast with those findings. Several factors may account for this difference. First, serpins competitively, but not completely, inhibit proteases. Second, in transgenic mice that express high levels of crmA throughout their whole lifespan, related cellular pathways are likely to compensate and activate the developmentally indispensable receptor-mediated apoptotic pathway. This is in line with the findings that caspase-9-deficient mice are viable (29, 30), and cells isolated from caspase-3 knock-out mice still undergo TNF- and staurosporine-mediated apoptosis (31). The equilibrium between apoptosis and survival, especially in acutely oxygen-underserved areas in ischemic settings, is tightly regulated. TAT-crmA

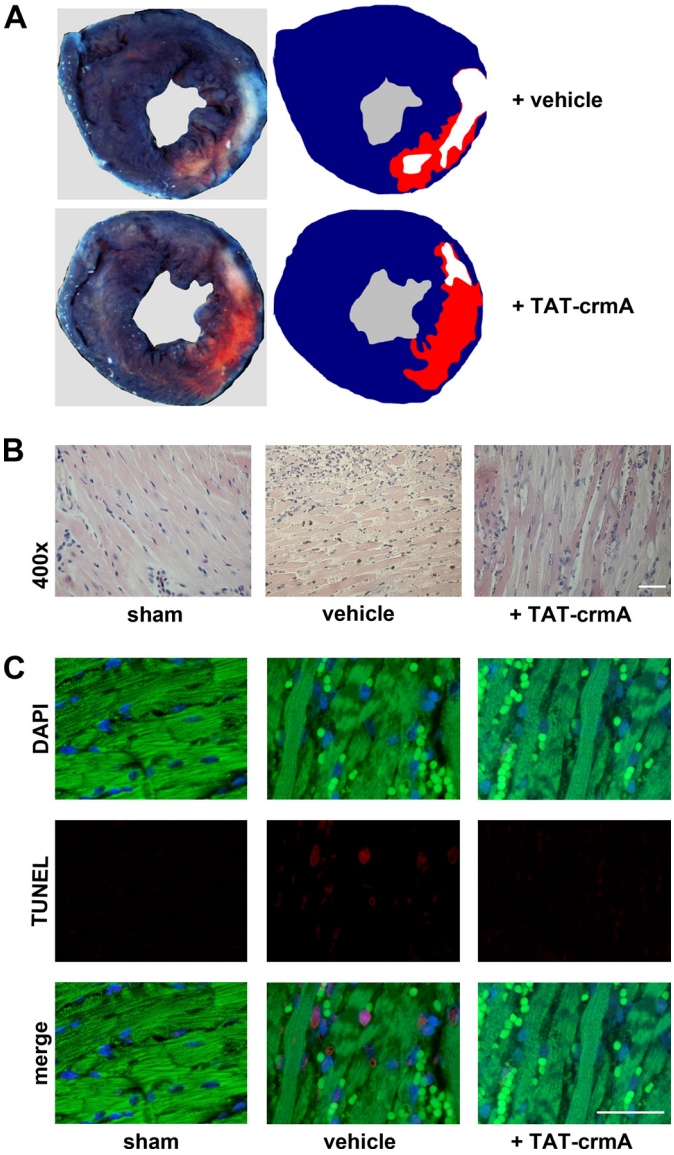

FIGURE 6. **TAT-crmA reduces myocardial tissue damage after LAD-ligation in mice.** *A*, mice were treated with vehicle or TAT-crmA and underwent transient LAD ligation for 1 h, followed by reperfusion for 24 h. Areas at risk and infarction sizes were determined by Evans blue and 2,3,5-triphenyltetrazolium chloride staining ($n = 18$). Representative cross-sections are shown. The area of the myocardium not stained with Evans blue represents the area at risk. Infarcted areas appear *pallid* while viable myocardium appears *pink*. *B*, histological evaluation of infarction size by H&E staining. Micrographs of sham-, vehicle-, and TAT-crmA-treated mice are shown. Distinguishable features of myocardial infarction, including vacuolization of cardiomyocytes, cell swelling, edema, and infiltration of granulocytes and mononuclear cells were significantly less pronounced in heart tissues obtained from TAT-crmA-treated mice compared with vehicle-treated tissues. *C*, apoptotic cardiomyocytes in the infarction border zone were detected by TUNEL staining (*red*). Nuclei are counterstained with DAPI (*blue*, *upper panel*). Autofluorescence of cardiomyocytes and erythrocytes appears *green*. *Bars* represent 50 μm.

TABLE 1
Analysis of cardiac function after LAD ligation

	Sham operation	TAT-crmA administration after ischemia		
		Vehicle	TAT-crmA	*p* value
Number of animals tested	3	13	13	
Body weight, g	23.2 (± 0.8)	24.0 (± 1.1)	24.0 (± 1.1)	0.47
Histology				
Area at risk, mm^2	0	36.9 (± 2.4)	35.4 (± 2.8)	0.33
Infarction size, mm^2	0	19.0 (± 1.4)	11.5 (± 1.2)	<0.001
Echocardiography				
Heart rate, bpm	445 (± 12)	434 (± 8)	417 (± 11)	0.12
Ejection fraction, %	71.0 (± 3.7)	23.2 (± 4.9)	39.3 (± 4.2)	0.002
LVESV, μl	15.3 (± 1.1)	53.3 (± 3.2)	39.6 (± 2.8)	0.003
LVEDV, μl	54.7 (± 3.1)	70.5 (± 2.4)	64.2 (± 2.8)	0.06

appears to shift the balance toward survival. From our studies, we cannot quantify the contribution of TAT-crmA to either the intrinsic or extrinsic pathway as they relate to protection of the reperfused heart. Because the apoptotic cross-talk between both pathways is complex, effective inhibition of general apoptosis in any ischemia-reperfusion injury may be obtained using an evolutionarily optimized viral multicaspase inhibitor rather than by selectively targeting defined pro-apoptotic proteins. Unlike TAT-crmA, single synthetic caspase inhibitors like z-VAD and others are cytotoxic already in low molecular range and will therefore not be able to enter clinical trials. We did not observe any cytotoxicity *in vivo* even if TAT-crmA was applied at ultra-high concentrations (daily intraperitoneal applications of 1 mg of TAT-crmA for 1 week; $n = 5$, data not shown).

Unlike many *in vitro* studies that investigated isolated pro-apoptotic pathways, blocking apoptosis should aim to comprehensively block multiple pro-apoptotic pathways, *e.g.* intrinsic, extrinsic, caspase-independent necroptosis, and possibly autophagy-associated cell death to gain maximal cell protection. In search for a broad blocker of apoptosis, viral anti-apoptotic proteins appear to outrange synthetic inhibitors as far as these compounds are analyzed.

In summary, blocking apoptosis has not yet become routine in clinical settings. More detailed knowledge about blocking apoptosis will be gained in the next decade to provide insights into the molecular pro-apoptotic pathways that are required on the way to preclinical trials with anti-apoptotic agents. However, TAT-crmA represents one candidate that is likely to meet the requirements for a clinically useful apoptosis inhibitor in the setting of ischemia-reperfusion injury and diseases that involve both the intrinsic and extrinsic apoptotic pathways.

Acknowledgments—We thank Katarina Stanke, Michaela Vorwerk, and Christian Willenbockel for excellent technical support.

REFERENCES

1. Hotchkiss, R. S., Strasser, A., McDunn, J. E., and Swanson, P. E. (2009) *N. Engl. J. Med.* **361,** 1570–1583
2. Krammer, P. H., Arnold, R., and Lavrik, I. N. (2007) *Nat. Rev. Immunol.* **7,** 532–542
3. Oberst, A., Bender, C., and Green, D. R. (2008) *Cell Death. Differ.* **15,** 1139–1146
4. Suliman, H. B., Carraway, M. S., Ali, A. S., Reynolds, C. M., Welty-Wolf, K. E., and Piantadosi, C. A. (2007) *J. Clin. Invest.* **117,** 3730–3741
5. Shelton, S. N., Shawgo, M. E., and Robertson, J. D. (2009) *J. Biol. Chem.* **284,** 11247–11255
6. Callus, B. A., and Vaux, D. L. (2007) *Cell Death. Differ.* **14,** 73–78
7. Miura, M., Friedlander, R. M., and Yuan, J. (1995) *Proc. Natl. Acad. Sci. U.S.A.* **92,** 8318–8322
8. Pop, C., Timmer, J., Sperandio, S., and Salvesen, G. S. (2006) *Mol. Cell* **22,** 269–275
9. Tewari, M., and Dixit, V. M. (1995) *J. Biol. Chem.* **270,** 3255–3260
10. Schwarze, S. R., Ho, A., Vocero-Akbani, A., and Dowdy, S. F. (1999) *Sci-*

ence **285,** 1569–1572
11. Toro, A., and Grunebaum, E. (2006) *J. Clin. Invest.* **116,** 2717–2726
12. Gustafsson, A. B., and Gottlieb, R. A. (2008) *Cardiovasc. Res.* **77,** 334–343
13. Rüdiger, H. A., and Clavien, P. A. (2002) *Gastroenterology* **122,** 202–210
14. Nogae, S., Miyazaki, M., Kobayashi, N., Saito, T., Abe, K., Saito, H., Nakane, P. K., Nakanishi, Y., and Koji, T. (1998) *J. Am. Soc. Nephrol.* **9,** 620–631
15. Martin-Villalba, A., Hahne, M., Kleber, S., Vogel, J., Falk, W., Schenkel, J., and Krammer, P. H. (2001) *Cell Death. Differ.* **8,** 679–686
16. Kempf, T., Eden, M., Strelau, J., Naguib, M., Willenbockel, C., Tongers, J., Heineke, J., Kotlarz, D., Xu, J., Molkentin, J. D., Niessen, H. W., Drexler, H., and Wollert, K. C. (2006) *Circ. Res.* **98,** 351–360
17. Krautwald, S., Ziegler, E., Tiede, K., Pust, R., and Kunzendorf, U. (2004) *J. Biol. Chem.* **279,** 44005–44011
18. Rabuffetti, M., Sciorati, C., Tarozzo, G., Clementi, E., Manfredi, A. A., and Beltramo, M. (2000) *J. Neurosci.* **20,** 4398–4404
19. Wiessner, C., Sauer, D., Alaimo, D., and Allegrini, P. R. (2000) *Cell Mol. Biol.* **46,** 53–62
20. Hotchkiss, R. S., and Nicholson, D. W. (2006) *Nat. Rev. Immunol.* **6,** 813–822
21. Tanaka, M., Ito, H., Adachi, S., Akimoto, H., Nishikawa, T., Kasajima, T., Marumo, F., and Hiroe, M. (1994) *Circ. Res.* **75,** 426–433
22. Meldrum, D. R. (1998) *Am. J. Physiol.* **274,** R577-R595
23. Li, Y., Takemura, G., Kosai, K., Takahashi, T., Okada, H., Miyata, S., Yuge, K., Nagano, S., Esaki, M., Khai, N. C., Goto, K., Mikami, A., Maruyama, R., Minatoguchi, S., Fujiwara, T., and Fujiwara, H. (2004) *Circ. Res.* **95,** 627–636
24. Gomez, L., Chavanis, N., Argaud, L., Chalabreysse, L., Gateau-Roesch, O., Ninet, J., and Ovize, M. (2005) *Am. J. Physiol. Heart Circ. Physiol.* **289,** H2153–H2158
25. Bhuiyan, M. S., Takada, Y., Shioda, N., Moriguchi, S., Kasahara, J., and Fukunaga, K. (2008) *Cardiovasc. Ther.* **26,** 10–23
26. Braunwald, E. (1989) *Circulation* **79,** 441–444
27. Sung, J. H., Zhao, H., Roy, M., Sapolsky, R. M., and Steinberg, G. K. (2007) *Neuroscience* **149,** 804–812
28. Kilic, E., Wippel, A., Kilic, U., Vogel, P., Kim, M., van der Putten, H., Wiessner, C., Rovelli, G., Böttiger, B. W., and Hermann, D. M. (2007) *Brain. Res.* **1185,** 293–300
29. Hakem, R., Hakem, A., Duncan, G. S., Henderson, J. T., Woo, M., Soengas, M. S., Elia, A., de la Pompa, J. L., Kagi, D., Khoo, W., Potter, J., Yoshida, R., Kaufman, S. A., Lowe, S. W., Penninger, J. M., and Mak, T. W. (1998) *Cell* **94,** 339–352
30. Kuida, K., Haydar, T. F., Kuan, C. Y., Gu, Y., Taya, C., Karasuyama, H., Su, M. S., Rakic, P., and Flavell, R. A. (1998) *Cell* **94,** 325–337
31. Jänicke, R. U., Sprengart, M. L., Wati, M. R., and Porter, A. G. (1998) *J. Biol. Chem.* **273,** 9357–9360